Pergamon

J. Mech. Phys. Solids, Vol. 42, No. 4, pp. 649–663, 1994
Elsevier Science Ltd
Printed in Great Britain
0022-5096/94 $6.00+0.00

CRACKING IN CERAMIC ACTUATORS CAUSED BY ELECTROSTRICTION

W. YANG† and Z. SUO‡

†Department of Engineering Mechanics, Tsinghua University, Beijing 100084, China; and
‡Mechanical and Environmental Engineering Department, University of California, Santa Barbara, CA 93106-5070, U.S.A.

(*Received* 21 *August* 1993; *in revised form* 23 *October* 1993)

ABSTRACT

MANY PEROVSKITE-TYPE ceramics deform appreciably under electric fields; they make good actuators which deliver motions upon receiving electrical signals. High electric fields are usually applied to induce large strains. Fracture has been observed in the actuators under electrical loading. In this theoretical study, the phenomenon is examined on the basis of electrostriction and fracture mechanics. Attention is focused on a crack emanating from an internal electrode or a conducting damage path. At the edge of the conducting path, the electric field is intense and nonuniform, inducing incompatible electrostrictive strains. Consequently, a stress field is set up in the ceramic, localized around the edge of the conducting path. The condition for the stress to extend a crack is estimated by two models, using either quadratic or step-like electrostriction law. It is found that, under a given electric field, cracking is suppressed in a multilayer actuator if the ceramic layers are sufficiently thin.

1. INTRODUCTION

SUBJECTED TO AN ELECTRIC FIELD, a dielectric crystal expands in the direction of the field, and contracts in the direction transverse to the field. If the crystal has a symmetry center, the strain state is unchanged when the electric field of the same magnitude is switched to the opposite direction. Thus, the strains vary approximately with the electric field squared. The phenomenon is called electrostriction. For most materials the electrostrictive strains are small, typically less than 10^{-7} at an electric field 1 MV m^{-1}, and therefore of little practical consequence. However, the same electric field can induce strains exceeding 10^{-3} in some perovskite-type oxides. These oxides make good actuators, delivering motions upon receiving electric signals (UCHINO, 1986). Because high electric field is required to induce a large strain, the actuators are usually made like multilayer capacitors with alternating oxides and electrodes, so that a modest voltage can induce an appreciable deflection (WINZER *et al.*, 1989).

One reliability issue has been raised recently (TAYLOR *et al.*, 1988; WINZER *et al.*, 1989). The electric field is intense and nonuniform around inhomogeneities such as inclusions and internal electrodes. The nonuniform electric field induces incompatible electrostrictive strains and thereby stresses. Crack growth under high electric field has been demonstrated experimentally (UCHINO and FURUTA, 1992; CAO *et al.*, 1993; LYNCH *et al.*, 1993). A frequently cited example is a crack emanating from an internal

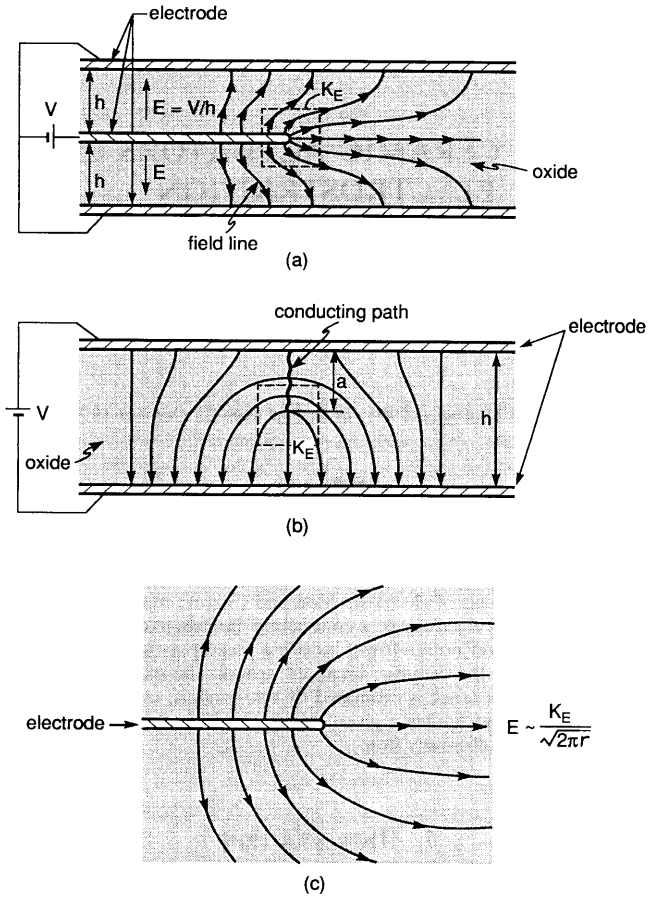

FIG. 1. Electric field concentration around the edge of a conducting sheet. (a) An internal electrode in a two layer actuator. (b) A conducting path growing from one electrode to another. (c) A half-plane conductor in an infinite dielectric.

electrode in multilayer actuators. Figure 1(a) illustrates a two-layer actuator. Each oxide layer is several tenths of a millimeter thick, and each electrode about a few microns thick. The two outside electrodes have the same electric potential, which differs from the potential on the middle electrode by V. The oxide far behind the edge of the middle electrode is subjected to a vertical electric field $\bar{E} = V/h$, but the oxide far ahead of the edge has negligible electric field. A stress field is therefore induced around the edge.

A second example is a conducting damage path growing in an oxide, striving to bridge the two electrodes [Fig. 1(b)]. The electrostrictive stress drives the crack; the crack, in turn, transports charged species available in the environment. A heuristic analysis of the phenomenon has been given by SUO (1993). Although the nature of the field concentration is similar to that at the electrode edge in Fig. 1(a), we are unaware of any controlled experiment on a conducting damage path.

Experimentally, the electrostrictive cracks are usually demonstrated under extreme conditions to accelerate the growth rate. A connection between these demonstrations and actuators in service is still unestablished. Exploring mechanisms by theoretical modeling will help to make such a connection. In this paper, a phenomenological description of electrostriction is first reviewed. In Section 3, the electric field near the edge of a conducting path is described, assuming small-scale nonlinearity. Two models are presented in Sections 4 and 5, respectively, using quadratic and step-like electrostriction.

2. Electrostriction

This section reviews experimental observations that lead to a constitutive law for electrostrictive ceramics suitable for field analysis. Representative data for a lead magnesium niobate $PbMg_{1/3}Nb_{2/3}O_3$ (PMN) based ceramic are listed in Table 1 as an illustration (Jang *et al.*, 1980; Winzer *et al.*, 1989). The materials are taken to be isotropic, so that data under uniaxial electric field and stress are applicable under multiaxial conditions. Typical results from three uniaxial tests are as follows. First, an electric field is applied in the absence of stresses. Because the material is isotropic, the electric displacement D is in the same direction as the electric field E. Hysteresis is negligible either at sufficiently high temperatures or with suitable doping. Thus, D varies reversibly with E; this nonlinear relation is written as

$$E = f(D). \tag{2.1}$$

As shown in Fig. 2(a), the curve is approximately linear at low fields, but the slope of the tangent decreases as the electric field increases. The slope at small fields defines the permittivity ε, i.e. $D = \varepsilon E$ as $E \to 0$. The nonlinearity plays important roles at the field concentration sites.

Second, in the absence of stresses, the electric field induces a longitudinal expansion and a transverse contraction. As reviewed by Sundar and Newnham (1992), to a high accuracy, the strains are proportional to the electric displacement squared [Fig. 2(b)]. Let the electric field coincide with the x_3-axis, and the three normal strains are written

$$\gamma_{33} = Q_{11} D_3^2, \quad \gamma_{11} = \gamma_{22} = Q_{12} D_3^2, \tag{2.2}$$

where Q_{11} and Q_{12} are the electrostrictive coefficients ($Q_{11} > 0$, $Q_{12} < 0$). Both Q_{11} and the ratio $q = -Q_{12}/Q_{11}$ are listed in Table 1. At small applied fields, the linearity between D and E renders γ proportional to the electric field squared, $\gamma = Q\varepsilon^2 E^2$.

Table 1. *Representative data for a high-electrostriction ceramic*

Material	$\varepsilon/\varepsilon_0$	Y (GPa)	ν	Q_{11} ($m^4\,C^{-2}$)	q	K_{Ic} ($MPa\sqrt{m}$)
0.9 PMN : 0.1 PT	7500	112	0.26	0.025	0.38	≈ 1

($\varepsilon_0 = 8.85 \times 10^{-12}$ F m^{-1}).

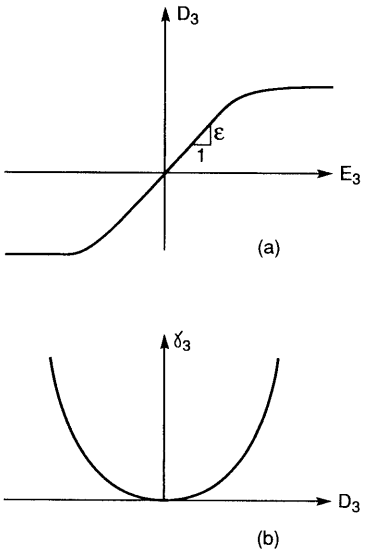

FIG. 2. Behaviors of electrostrictive ceramics. (a) Nonlinear but reversible relation between electric field and electric displacement. (b) Quadratic relation between electric displacement and electrostrictive strain.

However, the strain deviates from this relation when the electric field becomes large; see Fig. 3.

Third, in the absence of the electric field, stresses and strains obey Hooke's law. Under a uniaxial stress σ_{33}, the three strains are

$$\gamma_{33} = \sigma_{33}/Y, \quad \gamma_{11} = \gamma_{22} = -\nu\sigma_{33}/Y, \tag{2.3}$$

where Y is Young's modulus, and ν Poisson's ratio.

All the above can be described by a thermodynamic framework (e.g. LINES and GLASS, 1977). Let $u(s, \mathbf{D}, \gamma)$ be the internal energy per unit volume, s the entropy per

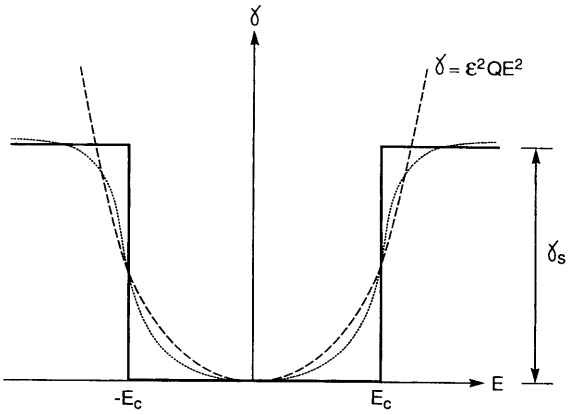

FIG. 3. Electrostrictive strain γ vs electric field E: quadratic electrostriction (dash), step-like electrostriction (solid) and the actual response (dot).

unit volume, **D** the electric displacement vector, and γ the strain tensor. For an increment of the state variables, the internal energy varies by

$$\mathrm{d}u = T\,\mathrm{d}s + E_i\,\mathrm{d}D_i + \sigma_{ij}\,\mathrm{d}\gamma_{ij}. \tag{2.4}$$

Here T is the temperature. The usual summation convention is adopted. More convenient to use is the elastic Gibbs free energy per unit volume $g(T, \mathbf{D}, \sigma)$, defined by

$$g = u - Ts - \sigma_{ij}\gamma_{ij}. \tag{2.5}$$

For a small increment in the variables, g varies by

$$\mathrm{d}g = -s\,\mathrm{d}T + E_i\,\mathrm{d}D_i - \gamma_{ij}\,\mathrm{d}\sigma_{ij}. \tag{2.6}$$

At a given temperature, g is a function of the electric displacements and stresses. Once the function $g(\mathbf{D}, \sigma)$ is prescribed, the electric fields and strains are obtained from

$$E_i = \partial g/\partial D_i, \quad \gamma_{ij} = -\partial g/\partial \sigma_{ij}. \tag{2.7}$$

The standard procedure is to write g in a power series of D_i and σ_{ij}, and retain the fewest terms that properly represent the experimental data. For isotropic electrostrictive ceramics, the function that describes the above experimental data is

$$g(\sigma, \mathbf{D}) = -\frac{1+\nu}{2Y}\left(\sigma_{ij}\sigma_{ij} - \frac{\nu}{1+\nu}\sigma_{mn}\sigma_{nn}\right) - (Q_{11}-Q_{12})\sigma_{ij}D_iD_j - Q_{12}\sigma_{mm}D_nD_n + \int_0^D f\,\mathrm{d}D. \tag{2.8}$$

Here $D = (D_nD_n)^{1/2}$ is the magnitude of the electric displacement. Like the elastic constants, the electrostrictive constants form a fourth-rank tensor; only two constants are independent for an isotropic material. Taking the differentiations (2.7), one obtains the three-dimensional constitutive equations

$$\gamma_{ij} = \frac{1+\nu}{Y}\left(\sigma_{ij} - \frac{\nu}{1+\nu}\sigma_{mm}\delta_{ij}\right) + (Q_{11}-Q_{12})D_iD_j + Q_{12}D_nD_n\delta_{ij}, \tag{2.9}$$

and

$$E_i = -2(Q_{11}-Q_{12})\sigma_{ij}D_j - 2Q_{12}\sigma_{mm}D_i + f(D)D_i/D, \tag{2.10}$$

where Kronecker's delta $\delta_{ij} = 0$ when $i \neq j$, and $\delta_{ij} = 1$ when $i = j$.

Combined with the standard field equations listed in Appendix A, these constitutive equations define a class of electrostriction problems. The field equations are linear but the constitutive equations are nonlinear, so their solutions are in general cumbersome. Nonetheless, the problem can be solved by the finite element method. The following observations simplify the analytical work in the subsequent sections.

In the absence of electrical loading, the problem reduces to a pure elasticity problem. This is because the vanishing electric fields and electric displacements satisfy (2.10) and the electrical field equations in Appendix A, as well as the homogeneous boundary conditions. Furthermore, the vanishing electric displacements reduce (2.9) to Hooke's law. However, the converse is not true. In the absence of mechanical loading, the

electrical loading will induce the electrostrictive strains. The electrostrictive strains are incompatible around inhomogeneities, so that stresses are induced to satisfy compatibility.

Equation (2.10) indicates that stresses can influence the electric field. However, such effects are small unless the stress field is appreciable. Consider a one-dimensional case

$$E = (-2Q\sigma + 1/\varepsilon)D. \tag{2.11}$$

The dielectric response is assumed to be linear. Taking the stress to be $\sigma = 10^7$ Pa, one finds that the first term in the bracket is less than 5% of the second.

The general solution procedure is as follows. First solve the electrostatic problem using a linear dielectric response

$$\mathbf{D} = \varepsilon \mathbf{E}. \tag{2.12}$$

The electrostatic strains are obtained from (2.9) and then prescribed in the elasticity problem. The procedure is much like thermal stress analysis, which is adopted in the earlier work by KNOPS (1963) in developing a complex variable method, and by WINZER *et al.* (1989) for a finite element method.

3. SMALL-SCALE NONLINEARITY

Figure 1(c) enlarges the zone near the edge of the conducting sheets, i.e. a conducting half-plane embedded in an infinite dielectric. The thickness of the conducting plane is small compared to the other dimensions in the device. No external mechanical loading is applied, so that stresses are negligible everywhere except for a small zone around the edge of the conducting sheet. The electric field is first determined by neglecting the stress term in (2.10), which will then be used as the external boundary condition to determine the near-edge stress field in the later sections. A formulation of this nature is suitable for the case of small-scale nonlinearity, in which the nonlinear regime obeying (2.1) is embedded within the field dominated by linear permittivity.

The electric field around the edge of a half-plane conductor can be found in standard electrostatics textbooks, which is determined from (2.12) and (A.4–6). Let (r,θ) be the polar coordinate centered at the edge of the half-plane. The electric field is

$$[E_1, E_2] = K_E(2\pi r)^{-1/2}[\cos(\theta/2), \sin(\theta/2)]. \tag{3.1}$$

The electric intensity factor K_E scales with the applied electric load; $K_E > 0$ corresponds to the tip accumulating the positive charges, and $K_E < 0$ the negative charges. Note that the magnitude of the field is independent of θ, given by

$$E = K_E(2\pi r)^{-1/2}. \tag{3.2}$$

The energy release rate is (SUO, 1993)

$$\mathcal{G} = \tfrac{1}{2}\varepsilon K_E^2. \tag{3.3}$$

This equation establishes that $\mathcal{G}$ and K_E are equivalent loading parameters.

The intensity factor K_E is related to the applied electrical loading and the device

geometry, which can be extracted from Fracture Mechanics handbooks. For the two-layer actuator in Fig. 1(a), the energy release rate is

$$\mathcal{G} = \varepsilon V^2/h. \tag{3.4}$$

Observe that the energy release rate is independent of the length of the conducting path. Thus, if the conducting path grows along the centerline, the growth rate should be constant. As a numerical example, consider an actuator with permittivity $\varepsilon = 5 \times 10^{-8}$ F m^{-1}, and thickness of each layer $h = 5 \times 10^{-4}$ m. An applied field $V/h = 10^6$ V m^{-1} provides an energy release rate $\mathcal{G} = 25$ J m^{-2} at the edge of the electrode. (The fracture energy of the perovskite-type ceramics under mechanical loading is around 10 J m^{-2}.) Complications may arise in practice; for example, an experiment by UCHINO and FURUTA (1992) shows that the crack tends to deviate from the centerline towards the two outside electrodes. An explanation for this crack path deviation might be furnished by utilizing the complete electric field solution.

Next consider the conducting path in Fig. 1(b). Similar cracks may be introduced by indentation and made conducting by applying a drop of an electrolyte. The energy release rate is given by

$$\mathcal{G} = (\varepsilon V^2/h) \tan(\pi a/2h). \tag{3.5}$$

Note that the energy release rate increases with the length of the conducting path. Consequently, the growth rate of the path at the constant voltage is expected to increase with the path length.

4. Quadratic Electrostriction

We now compute the stress field localized around the edge of the conducting sheet. Because of the complexity in the constitutive law, exact solutions consistent with every detail of the governing equations are difficult to obtain. Two models will be analysed in the following sections, each capturing some aspects of the problem. We first assume quadratic electrostriction, so that the D–E relation is linear and γ is quadratic in E (Fig. 3, dashed line). The stress terms in (2.10) are ignored. The plane strain conditions prevail. The general two-dimensional electrostriction problem was formulated by KNOPS (1963) in terms of complex potentials; his solution is recapitulated in Appendix B. This method was used by SMITH and WARREN (1966) for inclusions and cavities, and by MCMEEKING (1989) for insulating cracks. In what follows we use the method to determine the stresses at the edge of the conducting sheet, and assess whether the stresses will cause cracking.

The complex electric potential that describes the field (3.1) is

$$\Omega(z) = -K_E\sqrt{2z/\pi}. \tag{4.1}$$

Since the electric field is square-root singular, the strains and stresses must be $1/r$ singular, suggesting the following form for the Muskhelishivili potentials,

$$\varphi(z) = A \ln z, \quad \psi(z) = B \ln z. \tag{4.2}$$

The constants A and B are to be determined. In (4.1) and (4.2) the branch cut of functions $\sqrt{z}$ and $\ln z$ coincides with the conducting sheet.

The conducting sheet is assumed to be infinitely thin, so that displacements are continuous across the sheet, i.e.

$$(u_1 + iu_2)_{\theta=\pi} = (u_1 + iu_2)_{\theta=-\pi}. \tag{4.3}$$

The resultant forces on the two sides of the sheet are balanced, so that

$$(F_1 + iF_2)_{\theta=\pi} = (F_1 + iF_2)_{\theta=-\pi}. \tag{4.4}$$

The conditions (4.3) and (4.4), in conjunction with the basic relations in Appendix B, determine the two constants A and B. Thus,

$$\varphi(z) = \psi(z) = \frac{1+q}{16\pi} Y'\varepsilon^2 Q_{11} K_E^2 \ln z, \tag{4.5}$$

where $Y' = Y/(1-\nu^2)$ is the plane strain Young's modulus.

Stresses and displacements can be calculated using the basic formulas in Appendix B. In particular, the normal stress along the x-axis is

$$\sigma_{22} = \frac{1+q}{8\pi} Y'\varepsilon^2 Q_{11} \frac{K_E^2}{x}. \tag{4.6}$$

Note that σ_{22} is $1/x$ singular, tensile ahead of the edge and compressive behind. Incidentally, this distribution is similar to that due to a wedge or an edge dislocation inserted into a linear elastic solid.

We next examine whether this stress can cause cracking near the edge of the conducting sheet. A freshly nucleated crack is insulating before the charged species migrates into the crack. Since the electric field directly ahead of the edge is oriented in the x-direction, the electric field (3.1) is unperturbed by the crack. However, the stress field will be perturbed by the crack because the traction vanishes on the crack faces. The crack problem can be solved as follows. If the stress terms in (2.10) are ignored, any pure elastic problem can be superimposed on an electrostrictive problem. Now consider the superposition of the following two problems: (i) the electrostrictive problem without crack as just solved, and (ii) the pure elastic problem of a crack under pressure of the same magnitude as in (4.6). The latter gives the stress intensity factor K_I. Consequently, the crack of size a, emanating from the conducting sheet, has

$$K_I = \sqrt{\frac{1}{2\pi}} \frac{1+q}{4} Y'\varepsilon^2 Q_{11} \frac{K_E^2}{\sqrt{a}}. \tag{4.7}$$

The stress intensity factor K_I is quadratic with the electric intensity factor K_E, and inversely proportional to the square-root of the crack length. As the crack grows, K_I declines and the crack arrests when the fracture toughness K_{Ic} is reached. The situation is much like a Zener crack induced at the bottom of an edge dislocation pileup.

As an example of using (4.7), consider a crack emanating from the centerline electrode in Fig. 1(a). The electric field intensity factor K_E is obtained from (3.3) and (3.4), which gives $K_E = \bar{E}\sqrt{2h}$. The amount of crack growth is solved from (4.7):

$$a = (\beta h Y' \bar{\gamma}/K_{Ic})^2, \tag{4.8}$$

where

$$\beta = \frac{1+q}{2\sqrt{2\pi}}, \quad \bar{\gamma} = \varepsilon^2 Q_{11} \bar{E}^2. \tag{4.9}$$

The constant β ranges from 0.26 to 0.28. Note that the crack extension increases with the thickness of each layer in an actuator. For the typical case of $Y' = 120$ GPa, $\bar{\gamma} = 10^{-3}$ and $K_{Ic} = 1$ MPa$\sqrt{\text{m}}$, the stable crack size is predicted to be $a = 10$–100 μm for $h = 100$–300 μm. This prediction qualitatively agrees with the experimental data of UCHINO and FURUTA (1992).

Steady crack growth occurs if a charged species migrates onto the fresh crack faces. Consequently, the crack gradually transforms into a conducting path. The growing speed is controlled by the diffusion rate of the charged species, as well as the amplitude of the applied field. In this model, the sheet is assumed to be infinitely thin. For an electrode of finite thickness, (4.6) is correct at a distance of a few thicknesses away from the electrode edge; the stress should be high but finite as the rounded electrode edge is approached. For a steadily growing conducting path, the electric field near the crack front may be affected by the field needed to transport the charged species. In either case, K_I should be finite for short cracks. The stress terms in (2.10) can be significant for high permittivity materials, which is ignored in our calculation. The significance of these issues remains to be assessed by controlled experiments and rigorous numerical analysis.

5. STEP-LIKE ELECTROSTRICTION

The quadratic electrostriction model in the preceding section disregards the nonlinearity of the D–E curve at high electric fields. The model overestimates the electrostriction effect on cracking immediately ahead of the electrode edge. In this section a step-like electrostriction is adopted. As shown in Fig. 3, the quadratic and the step-like electrostriction form bounding cases which provide insight into the actual response. In this section, we assume that an electric field E induces a step-like strain in the field direction:

$$\gamma = \begin{cases} \gamma_s, & |E| > E_c \\ 0, & |E| < E_c \end{cases}. \tag{5.1}$$

This description embodies two important quantities. The electrostriction becomes substantial when the electric field exceeds a certain level, the coercive field E_c; the electrostrictive strain attains a saturation value γ_s at large electric field. The strain transverse to the electric field direction is $-q\gamma$. With proper interpretation, the model presented below applies to materials with large hysteresis, such as ferroelectric and antiferroelectric ceramics.

From (3.1), the magnitude of the field decays with r according to $E = K_E(2\pi r)^{-1/2}$

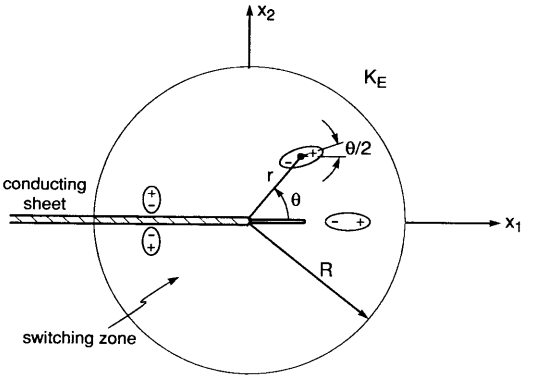

FIG. 4. Schematics of electrostriction near the edge of a conducting sheet. The poling direction is horizontal at $\theta = 0$, and vertical at $\theta = \pm\pi$.

in the region outside the nonlinear zone. The radius R within which the electrostriction is switched on is estimated by letting $E = E_c$. Thus,

$$R = \frac{1}{2\pi}(K_E/E_c)^2, \tag{5.2}$$

provided that switching does not alter the electric field. For a given material, R increases with applied load K_E squared. Inside the circle, the orientation of the electrostrictive strain is determined by the pre-switching electric field direction at each point:

$$\gamma_{ij} = \gamma_s[(1+q)\hat{E}_i\hat{E}_j - (1+v)q\delta_{ij}]. \tag{5.3}$$

Here $\hat{\mathbf{E}}$ is the unit vector tangent to the field line, given by (3.1). No electrostriction occurs outside the circle. The above features of electrostriction are shown schematically in Fig. 4.

This strain field is incompatible, so that a stress field is induced near the edge of the conducting sheet. The stress field is analysed in Appendix C. The hoop stress is given by

$$\sigma_{\theta\theta} = Y'\gamma_s\left[-\frac{1-(1+2v)q}{4} + \frac{1+q}{3}\cos\theta\right] \quad \text{for} \quad r < R,$$

$$\sigma_{\theta\theta} = Y'\gamma_s\left[\frac{1-(1+2v)q}{4}\frac{R^2}{r^2} - \frac{1+q}{6}\frac{R^3}{r^3}\cos\theta\right] \quad \text{for} \quad r > R. \tag{5.4}$$

The normal stress along the x-axis, which is bounded everywhere, is plotted in Fig. 5. It is tensile immediately ahead of the electrode tip and compressive right behind it. The abrupt changes of hoop stress across the switching boundary are due to the step-like electrostriction model.

We next discuss possible cracking ahead of the electrode. By releasing the holding traction along the cracking portion of electrode axis, the stress intensity factor is

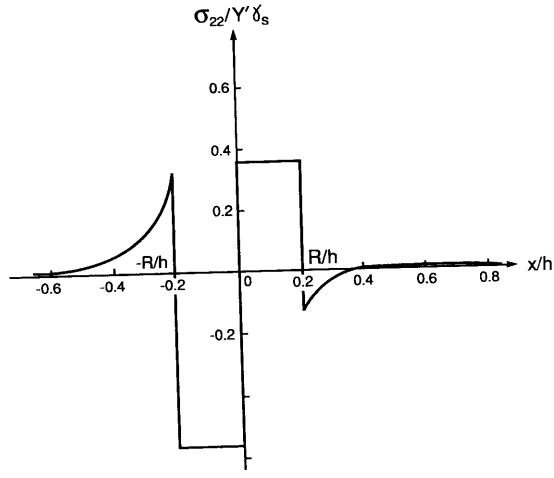

FIG. 5. Stress distribution along the x-axis under step-like electrostriction; $v = 0.26$, $q = 0.38$, $\bar{E}/E_c = 0.8$.

$$K_I = \sqrt{\frac{2}{\pi a}} \int_0^a \sqrt{\frac{x}{a-x}}\, \sigma_{22}(x)\, dx. \tag{5.5}$$

K_I versus a curve under step-like electrostriction is plotted in Fig. 6. Due to the sudden sign switch of holding traction at $r = R$, K_I maximizes when the crack reaches the poling boundary. This maximum value of K_I is

$$(K_I)_{max} = \alpha K_E Y' \gamma_s / E_c, \tag{5.6}$$

where

$$\alpha = \frac{1+(7+6v)q}{24}, \tag{5.7}$$

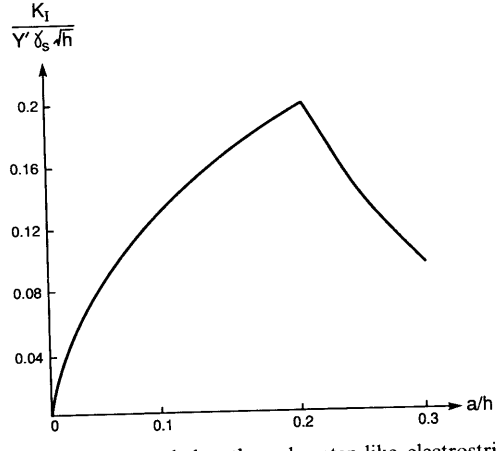

FIG. 6. Stress intensity factor versus crack length under step-like electrostriction; $v = 0.26$, $q = 0.38$, $\bar{E}/E_c = 0.8$.

and its value is around $\alpha \approx 0.18$. In contrast to the case of quadratic electrostriction, the crack may not nucleate instantaneously at the edge of conducting sheet; however, a tunnelling mechanism described by SUO (1993) could assist the cracking. The length of the crack scales with the switching zone size R.

For the centerline electrode in Fig. 1(a), the intensity factor is $K_E = \bar{E}\sqrt{2h}$. Furthermore, the dependence of $(K_I)_{max}$ on the applied field strength and the layer thickness appears to be less strong than the quadratic electrostriction case. The value of $(K_I)_{max}$ can be estimated as follows. Let us take $Y' = 120$ GPa, $\gamma_s = 0.002$, $\bar{E}/E_c = 0.8$ and $h = 300$ μm; then $(K_I)_{max} = 0.85$ MPa$\sqrt{\text{m}}$, falling in the range of the fracture toughness of perovskite-type ceramics.

Either quadratic or step-like electrostriction would provide estimates for cracking behavior ahead of a conducting sheet. The quadratic electrostriction model is pertinent for the case of long crack, in which the perturbation by nonlinear zone is far away from the crack tip. For relatively small a, on the other hand, the constitutive response near the crack tip or the electrode edge can be better characterized by the saturation of electrostrictive strain, thus justifying the step-like electrostriction model.

6. CONCLUDING REMARKS

Electric field induced fracture in ceramic actuators is attributed to electrostrictive strains. Such strains are incompatible around inhomogeneities, leading to stresses. Two models are analysed to estimate the magnitude of the stress and the extent to which it is localized. The estimates, in conjunction with a fracture mechanics analysis, allow us to establish the critical conditions. For a multilayer actuator subjected to a given electric field in each ceramic layer, cracking is suppressed if each layer is sufficiently thin. The models are also interpreted for a steadily growing damage path in a ceramic. The electric field induces electrostrictive stresses which drive the crack, and the crack transports charged species which extend the conducting path. Further progress in this area will be made by more rigorous numerical calculations and better controlled experiments.

ACKNOWLEDGEMENTS

The work of W. Yang was supported by a visiting appointment at the University of California, Santa Barbara, funded by ONR through contract N00014-93-1-0110, and by the National Natural Science Foundation of China. The work of Z. Suo was supported by NSF through grant MSS-9258115, and by ONR through contract N00014-93-1-0110.

REFERENCES

CAO, H. C., HE, M.-Y. and EVANS, A. G. (1993) Electric field-induced fatigue crack extension in ferroelectric ceramics. Submitted for publication.

JANG, S. J., UCHINO, K., NOMURA, S. and CROSS, L. E. (1980) Electrostrictive behavior of lead magnesium niobate based ceramic dielectrics. *Ferroelectrics* **27**, 31–34.

KNOPS, R. J. (1963) Two-dimensional electrostriction. *Qt. J. Mech. Appl. Math.* **16**, 377–388.

LINES, M. E. and GLASS, A. M. (1977) *Principles and Applications of Ferroelectrics and Related Materials*. Clarendon Press, Oxford.
LYNCH, C. S., CHEN, L., YANG, W., SUO, Z. and MCMEEKING, R. M. (1993) Crack growth in ferroelectric ceramics driven by cyclic polarization switching. In *Proceedings of Adaptive Structures and Material Systems Symposium* (ed. G. CARMAN and E. GARCIA). ASME, New York.
MAL, A. K. and SINGH, S. J. (1991) *Deformation of Elastic Solids*. Prentice Hall, New Jersey.
MCMEEKING, R. M. (1989) Electrostrictive stress near crack-like flaws. *J. Appl. Math. Phys.* **40,** 615–627.
Smith, T. E. and WARREN, W. E. (1966) Some problems in two-dimensional electrostriction. *J. Math. Phys.* **45,** 45–51; **47,** 109–110 (1968) (corrigenda).
SUNDAR, V. and NEWNHAM, R. E. (1992) Electrostriction and polarization. *Ferroelectrics* **135,** 431–446.
SUO, Z. (1993) Models for breakdown-resistant dielectric and ferroelectric ceramics. *J. Mech. Phys. Solids* **41,** 1155–1176.
TAYLOR, D. J., NEWNHAM, R. E. and CARLSON, W. B. (1988) The effect of electric field on mechanical strain and stress in flawed electroceramics. *Ferroelectrics* **87,** 81–84.
UCHINO, K. (1986) Electrostrictive actuators: materials and applications. *Am. Ceram. Soc. Bull.* **65,** 647–652.
UCHINO, K. and FURUTA, A. (1992) Destruction mechanism of multilayer ceramic actuators. *Proc. ISAF 1992*, Greenville, South Carolina, pp. 195–198.
WINZER, S. R., SHANKAR, N. and RITTER, A. P. (1989) Designing cofired multilayer electrostrictive actuators for reliability. *J. Am. Ceram. Soc.* **72,** 2246–2257.

APPENDIX A: BASIC FIELD EQUATIONS

The basic field equations are summarized here. Let $\mathbf{u}$ be the displacement vector and γ the strain tensor. Geometric compatibility requires that

$$\gamma_{ij} = \tfrac{1}{2}(u_{i,j} + u_{j,i}). \tag{A.1}$$

Equilibrium requires that the stress tensor σ satisfy inside a material

$$\sigma_{ij,i} = 0, \tag{A.2}$$

and jumps across an interface between two dielectrics by

$$n_i[\sigma_{ij}^{+} - \sigma_{ij}^{-}] = t_j, \tag{A.3}$$

where $\mathbf{n}$ is the unit normal to the interface pointing from the medium labeled as $+$, and $\mathbf{t}$ the traction applied on the interface. The body force is negligible.

The electric field vector $\mathbf{E}$ is related to the potential ϕ by

$$E_i = -\phi_{,i}. \tag{A.4}$$

The electric displacement vector $\mathbf{D}$ satisfies in a dielectric

$$D_{i,i} = 0, \tag{A.5}$$

and jumps across an interface by

$$n_i[D_i^{+} - D_i^{-}] = -\omega \tag{A.6}$$

where ω is the density of the free charge on the interface. The free charge inside the body is neglected.

APPENDIX B: COMPLEX VARIABLE FORMULATION FOR TWO-DIMENSIONAL ELECTROSTRICTION PROBLEMS

The formulation of two-dimensional electrostriction problems by KNOPS (1963) is summarized here. For a linear dielectric, the two-dimensional electric field is solved by a complex potential $\Omega(z)$:

$$-E_1+iE_2=\Omega'(z). \tag{B.1}$$

Here $z=z_1+ix_2$, and $i=\sqrt{-1}$. The effect of the stress due to the coupling term in (2.10) is taken to be negligible.

Equilibrium is satisfied by the introduction of Airy's function Φ

$$\sigma_{ij}=\nabla^2\Phi\delta_{ij}-\Phi_{,ij}. \tag{B.2}$$

The indices now range from 1 to 2. Under the plane strain conditions, (2.9) becomes

$$\gamma_{ij}=\frac{1+\nu}{Y}[(1-\nu)\nabla^2\Phi\delta_{ij}-\Phi_{,ij}]+\varepsilon^2(Q_{11}-Q_{12})E_iE_j+(1+\nu)\varepsilon^2Q_{12}E_mE_m\delta_{ij}. \tag{B.3}$$

The linear permittivity law (2.12) is also used. Compatibility for the above strain field leads to an inhomogeneous biharmonic equation

$$\nabla^4\Phi=-8S\Omega''(z)\overline{\Omega''(z)}, \tag{B.4}$$

where

$$S=\frac{1-(1+2\nu)q}{4}Y'\varepsilon^2Q_{11}. \tag{B.5}$$

The general solution to (B.4) consists of a homogeneous solution and a particular solution. The former is given by the classical Muskhelishivili potentials φ and ψ. A particular solution is $\Phi=-\frac{1}{2}S\Omega(z)\overline{\Omega(z)}$. The stresses, displacements and resultant forces are given by

$$\frac{\sigma_{11}+\sigma_{22}}{2}=\varphi'(z)+\overline{\varphi'(z)}-S\Omega'(z)\overline{\Omega'(z)} \tag{B.6}$$

$$\frac{\sigma_{22}-\sigma_{11}}{2}+i\sigma_{12}=\bar{z}\varphi''(z)+\psi'(z)-S\Omega''(z)\overline{\Omega(z)} \tag{B.7}$$

$$\frac{Y}{(1+\nu)}(u_1+iu_2)=(3-4\nu)\varphi(z)-z\overline{\varphi'(z)}-\overline{\psi(z)}+S\Omega(z)\overline{\Omega'(z)}+S_1\int\overline{\Omega'(z)^2}\,dz \tag{B.8}$$

$$F_1+iF_2=-i[\varphi(z)+z\overline{\varphi'(z)}+\overline{\psi(z)}-S\Omega(z)\overline{\Omega'(z)}] \tag{B.9}$$

where

$$S_1=\frac{1+q}{2(1+\nu)}Y\varepsilon^2Q_{11}. \tag{B.10}$$

APPENDIX C: STEP-LIKE ELECTROSTRICTION

The multiaxial formulation of step-like electrostriction can be proceeded in a way parallel to the derivation of (B.3). Anticipated in a small-scale switching situation, the electrostrictive strain, developed progressively from the electrode tip, always jumps a prescribed amplitude γ_s and aligned to the electric field when the switching zone swept by. The above heuristic reasoning leads to a phenomenological electrostriction law:

$$\gamma_{ij}=\frac{1+\nu}{Y}[(1-\nu)\nabla^2\Phi\delta_{ij}-\Phi_{,ij}]+\gamma_s[(1+q)\hat{E}_i\hat{E}_j-(1+\nu)q\delta_{ij}]. \tag{C.1}$$

We also assumed in Section 3 that the electric field is only slightly perturbed by the presence of a small nonlinear zone. Utilizing the electric field (3.1), one is able to phrase the compatibility equation as

$$\nabla^4\Phi + \frac{1+q}{2} Y'\gamma_s \frac{\cos\theta}{r^2} = 0. \tag{C.2}$$

The characteristics of the electrostriction under the present formulation can be examined by the following expressions of polar strain and displacement components

$$\gamma_{\theta\theta}+\gamma_{rr} = \frac{(1+v)(1-2v)}{Y}\nabla^2\Phi + \gamma_s[1-(1+2v)q]$$

$$\gamma_{\theta\theta}-\gamma_{rr} = \frac{1+v}{Y}\left[\frac{\partial^2}{\partial r^2} - \frac{\partial}{r\,\partial r} - \frac{\partial^2}{r^2\,\partial\theta^2}\right]\Phi - \gamma_s(1+q)\cos\theta$$

$$\gamma_{r\theta} = -\frac{1+v}{Y}\frac{\partial}{\partial r}\left(\frac{\partial\Phi}{r\,\partial\theta}\right) - \gamma_s\frac{1+q}{2}\sin\theta, \tag{C.3}$$

$$u_r = -\frac{1+v}{Y}\Phi_{,r} + \frac{r}{Y'}\Psi_{,\theta} + \frac{\gamma_s r}{2}[1-(1+2v)q+(1+q)\cos\theta]$$

$$u_\theta = -\frac{1+v}{Yr}\Phi_{,\theta} + \frac{r^2}{Y'}\Psi_{,r} - \gamma_s r(1+q)\sin\theta. \tag{C.4}$$

In the above expressions, terms associated with γ_s disappear outside the switching zone. The supplementary potential Ψ for the displacements relates to Φ by (e.g. MAL and SINGH, 1991)

$$\nabla^2\Psi = -\frac{Y'\gamma_s(1+q)}{2r^2}\sin\theta \quad (r\Psi_{,\theta})_{,r} = \nabla^2\Phi. \tag{C.5}$$

The other field equations, as well as the remaining boundary and continuity conditions, are homogeneous. The inhomogeneous terms in (C.2–5) reveal the salient features of solution. The Airy stress function should be the superposition of two terms

$$\Phi(r,\theta) = \Phi_H(r) + \Phi_0(r)\cos\theta. \tag{C.6}$$

The first term characterizes the axisymmetric field induced by the jump of mean electrostriction across $r = R$, whereas the second term takes into account the variation of poling directions near the electrode tip. The resolution for each term is complemented by the continuity requirements of tractions and displacements across $r = R$, and the asymptotic behaviors of stresses near the electrode tip and toward infinity. The field induced by the jump of mean electrostriction is solved by

$$\Phi_H = -\frac{Y'\gamma_s}{8}[1-(1+2v)q]r^2 \qquad \text{for } r < R$$

$$\Phi_H = -\frac{Y'\gamma_s}{4}[1-(1+2v)q]R^2\ln r \quad \text{for } r > R, \tag{C.7}$$

which corresponds to an axisymmetric and compressive stress field within the poling zone and a tensile hoop stress decaying like $1/r^2$ outside. Such a solution represents the stress field due to mean electrostriction averaged within the poling zone. Induced by the variation of poling directions within the switched zone, on the other hand, the second term in (C.6) can be solved by

$$\Phi_0 = \frac{1+q}{6}Y'\gamma_s r^2 \qquad \text{for } r < R$$

$$\Phi_0 = -\frac{1+q}{12}Y'\gamma_s\frac{R^3}{r} \quad \text{for } r > R. \tag{C.8}$$